CEAS-GNC-2022-014

CEAS EuroGNC 2022
"Conference on Guidance, Navigation and Control"
3-5 May 2022 @ Technische Universität Berlin, Germany

Procedural Minor Body Generator Tool for Data-Driven Optical Navigation Methods

Carmine Buonagura Research Assistant, Politecnico di Milano, Department of Aerospace Science and Technology, 20156, Milan, Italy. carmine.buonagura@polimi.it

Mattia Pugliatti PhD Student, Politecnico di Milano, Department of Aerospace Science and Technology, 20156, Milan, Italy. mattia.pugliatti@polimi.it

Francesco Topputo Full Professor, Politecnico di Milano, Department of Aerospace Science and Technology, 20156, Milan, Italy. francesco.topputo@polimi.it

ABSTRACT

Minor bodies show great variability in shape and surface morphological features. Since in the proximity of these bodies the dynamic is highly non-linear, communication windows with Earth could not be sufficient to navigate around them. Moreover, there is a growing demand for the reduction of costs deriving from ground-stations operations. As a result, the need for spacecraft with autonomous navigation capabilities both in far and close ranges. The most promising navigation technique is the optical one which allows the estimation of state information by exploiting optical observables extracted from images. To assess the robustness of optical navigation methods, it is required to perform tests on a variety of body shapes and with different surface morphological features. The importance of these tests arises from the shape and surface morphology estimation errors of ground-based estimation techniques. In this work, a procedural minor body generator tool implemented with an open-source 3D computer graphics software is described. The starting point of the tool is the three–dimensional mesh of a generic minor body which is procedurally modified by introducing craters, boulders, and surface roughness to obtain a photorealistic model in a real-looking environment. Two families of models can be generated by default: rocky ones, characterized by a large number of different-sized boulders, and cometary ones characterized by the typical morphology of comets, consisting of alternating rough and smooth regions, with the presence of small boulders.

Keywords: Asteroid; Small–body; Procedural; Generation; Data-driven

1 Introduction

Minor bodies exploration is an expanding field because these bodies give incomparable information on the solar system formation and evolution, they pose a constant threat to Earth, and they are a source of precious materials that could be exploited [1]. Up until now, several missions such as Osiris-Rex [2], Rosetta [3], Hayabusa 1 [4], and 2 [5], Lucy [6], and DART [7] have been launched towards these targets, while others, such as Hera [7] with its two CubeSats, Milani [8] and Juventas [9], and M-ARGO [10], are planned for the future.

In the context of far and close range applications, the spacecraft dynamics is highly non-linear, thus, its maneuvers must be precise to keep it along the nominal trajectory. Indeed, a small maneuver delay can cause a large offset from the designed trajectory. Autonomous navigation is pushing forward to release space exploration from the costs and constraints of ground-based operations.

Optical navigation is the most promising technique to autonomously navigate around minor bodies [1]. It is based on the processing of optical data taken by the onboard camera, followed by a filtering procedure that allows reconstructing the spacecraft state. The image processing (IP) performances strongly depend on the shape and surface morphological features of the small-body, such as craters and boulders. This implies that such methods have to be robust to these kinds of uncertainty. The uncertainty arises because minor bodies, such as asteroids and comets, are characterized by great variability in terms of shape and surface features which are difficult to estimate from ground-based observations. As reported in [11], light curve analysis is the simplest way to estimate minor bodies shape and it is based on the observation of their light curves. Practically, photometric observations of a body sampled over an extended period are used to measure the variation in the reflected light to get information on the shape. Most available 3D models are based on this technique, which provides a rough approximation. On the other hand, radar range-doppler imaging can be used for bodies that pass close to Earth as it exploits radio telescopes. This method allows achieving higher accuracy with respect to the aforementioned one in shape and spin estimation. A further technique is high-resolution imagery, exploiting a combination of images taken at different viewing geometries and phase angles. This method is used during rendezvous and flyby missions, and it is the most accurate, achieving uniform resolutions. Flyby targets cannot often have global shape reconstruction, due to the limited observation time and constrained geometry. The shape of the body is an important parameter to select the best performing visual based navigation (VBN) method, which has to be robust due to the estimation uncertainty [12]. The robustness of the processing techniques can be accessed by testing them on a large variety of different shapes and surface features, which results in the need for large images datasets. Moreover, data-driven methods, such as artificial intelligence techniques, are increasingly spreading and they constantly demand more data for training, validation, testing, and generalization purposes [13].

Different computer graphics software are available to model and render minor bodies. High-fidelity rendering engines such as ESA's PANGU [14], and Airbus Defence & Space's SurRender [15] are limited by software licenses. On the other hand, software such as POV-Ray[1] and Blender[2] are open-source but not specifically designed for rendering of celestial objects. The main difference between the last two is that Blender is well documented, supports Python scripting, and has a stronger community. This is why it has been selected in this work. Nonetheless, realistic minor bodies can be manually generated in Blender with great effort. For this reason, a Python code is built to generate the same results in fewer steps and in a procedural way. To realize it, the Blender/Python API is exploited, indeed, Blender embeds a Python interpreter provided by the "bpy" module that can be imported in a script and gives access to Blender data, classes, and functions. In this way, it is possible to access by script all the Blender functionalities.

This work presents a procedural minor body generator tool designed by the Deep-space Astrodynamics Research & Technology[3] (DART) group and it is used to support the validation and testing of IP and VBN algorithms as well as to construct datasets for artificial intelligence applications. In this context, in

[1] `http://www.povray.org/` Last access: January 19, 2022

[2] `https://www.blender.org/` Last access: January 19, 2022

[3] `https://dart.polimi.it/` Last access: January 19, 2022

[16], a showcase of the capabilities of the tool to generate a variety of bodies and surface characteristics has been fundamental to generate a dataset for semantic segmentation purposes.
The starting point of the tool is a small-body three-dimensional model whose shape can be rough or quite accurate depending on the observation technique used to recreate it. Thus, the important result achieved with this tool is the possibility to procedurally change surface features to generate a real-looking minor body. Furthermore, only a few small-bodies have been closely observed and faithfully reconstructed, such as Bennu and comet 67P. The tool allows generating models with realistic surface morphologies that can be used to validate and test algorithms. Moreover, there are two default surface morphology features that the tool can recreate. Firstly, a highly rocky body, such as Bennu, that presents an elevated number of boulders of different sizes [17]. Secondly a comet-like surface morphology, with the alternation of rough regions of rocks and smooth sand ones like 67P [18], with the presence of small boulders evenly distributed on the body surface.
The paper is structured as follows. Section 2 reports a brief explanation of the procedural operations considered to modify the original model. In this section, a short overview of the background environment, the rendering settings, and the possibility to introduce optical aberrations is also provided. In Section 3, a sample of results that can be achieved with the tool are presented, along with its validation with an image taken in the Rosetta mission. Some final considerations are then discussed in Section 4.

2 Methodology

The work aims to create a tool for the procedural generation of minor bodies to create high-fidelity images. Datasets can be easily built and exploited to validate and test the robustness of IP and VBN algorithms as well as to train, validate, and test data-driven methods. In the following sections, the procedure used for the generation of realistic surface morphological features is presented. The procedure starts from a rough small-body model and terminates with the real-looking minor body after its procedural modification.

2.1 Model Refinement

Above all, a model object is taken from existing databases [4, 5] and imported in Blender. The starting model can be rough or quite accurate depending on the observation technique used to recreate the model. In this step, it is important that the model does not exhibit mesh artifacts, resulting in a non-regular mesh distribution, as shown in Fig. 1. To take advantage of the same settings for all the models imported in the tool and to reduce computational effort, they are resized to the same average size, inscribing them in a 1m sphere. To generate a realistic rocky surface it is first required to smooth the mesh of the starting model. To accomplish this task the *subdivision surface* modifier[6] has been exploited twice. Its function is to split each primitive polygon contained in the mesh, increasing the vertices number of the model giving it a smooth appearance. The Catmull-Clark [19] subdivision method is used to accomplish this task by constructing new vertices based upon the average of the original points. After these modifiers have been applied the *smooth shading* functionality is used to reach a further smoothness. Fig. 2 shows the model surface improvements after applying the aforementioned modifiers. For models with large number of vertices, like comet 67P and asteroid Itokawa, shown in Fig. 3, there is no need to use modifiers as they are already highly accurate. If these modifiers are still used, the computational effort to apply them may exceed the available computational power. A possible solution to this problem and to reduce the rendering times, discussed later in Section 2.3.2, is to firstly use a *decimate modifier* in order to reduce the number of faces. The modifier leads to models whose shape is comparable to that of highly accurate ones and effectively reduces rendering time. The drawback is a significant increase in computational

[4] `https://astro.troja.mff.cuni.cz/projects/damit/asteroids/browse` Last access: January 20, 2022
[5] `https://sbn.psi.edu/pds/shape-models/` Last access: January 20, 2022
[6] `https://docs.blender.org/api/blender_python_api_2_77_0/info_overview.html` Last access: January 20, 2022

Fig. 1 Three dimensional model visual representation of asteroid Lutetia (left) and wireframe representation with mesh artifacts in Blender (right).

Fig. 2 Progressive mesh improvement of the model after subdivision surface modifiers are applied.

Fig. 3 From left to right there are minor bodies with an increasing number of faces. On the left asteroid Lutetia (512 faces), in the middle asteroid Itokawa (49,151 faces) and on the right comet 67P (1,309,996 faces)

time due to the high cost of faces reduction. As a result, for models with an arbitrary number of vertices higher than 10,000 only *smooth shading* is applied. Concerning models with a low count of faces, as Lutetia in Fig. 3, the *decimate modifier* effectively reduces the computational times. In this case, the final model will be smoother with a less realistic distribution of shadows, especially along the terminator resulting in a segmented line, as illustrated in Fig. 4. Since the saved time is not significant compared to the realism of the final model this modifier has been discarded.

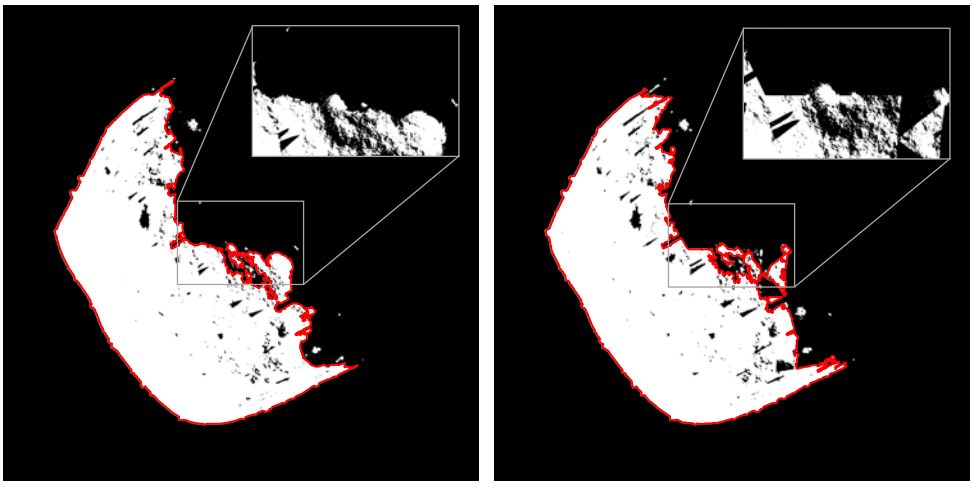

(a) **(b)**

Fig. 4 Binarized image of Bennu asteroid generated with and without the decimate modifier. (a) Model with 98,304 faces. (b) Model with 768 faces.

2.2 Surface Morphology

Surface morphology is the most important aspect in order to have a model visually resembling a minor body. As a result, it is important to modify its surface introducing morphological features such as roughness, craters, and boulders. A material is applied to the object to achieve a rough surface with craters, while boulders are physical three-dimensional objects randomly scattered across the surface.

2.2.1 Surface Roughness

The surface roughness is the first step in order to accomplish real-looking minor bodies. The material is applied to the model mesh exploiting the node tree available in the *shading editor* in Blender. First of all, to break uniformity of the color, a *noise* texture is inserted as illustrated in Fig. 5. The *noise* texture is then fed into a *bump* node that allows to normally displace the surface of the object in order to recreate the typical roughness of rocky bodies.

(a) **(b)**

Fig. 5 Surface roughness generation. (a) Noise texture applied on the model. (b) Displacement of the surface exploiting the bump node.

2.2.2 Craters

Craters are depressions made by impact events and are characterized by a rough circular shape. The shape is the result of the ejection of material in all directions after impact. These features are generated from the *voronoi* texture, characterized by multiple circles. To get the effect of an excavation, a *color ramp* node has been added with four different shades of black. It is then required to combine this texture with the surface roughness one. This is the reason why the *mix* node has been used. It works on the individual and corresponding pixels of the two input textures as reported in [7]. The main problem to solve is given by the protraction of the nearby roughness features inside the crater. Thus, the first operation performed is the subtraction of the craters texture from the surface roughness one. The result is a texture that presents the same pattern of the surface roughness one, but with white circles distributed on it. In order to give the impression of an excavation the craters must be black so that the software moves them towards the inner part of the model. Therefore, a multiplication is performed between the previously generated texture and the craters one. As described above, the *bump* node is exploited to move the surface of the object and recreate a realistic rough surface with craters on it. This approach can be performed different times in the node tree starting from different sizes *voronoi* textures to generate overlapping craters of different sizes and positions. The procedure followed for the craters generation is shown in Fig. 6.

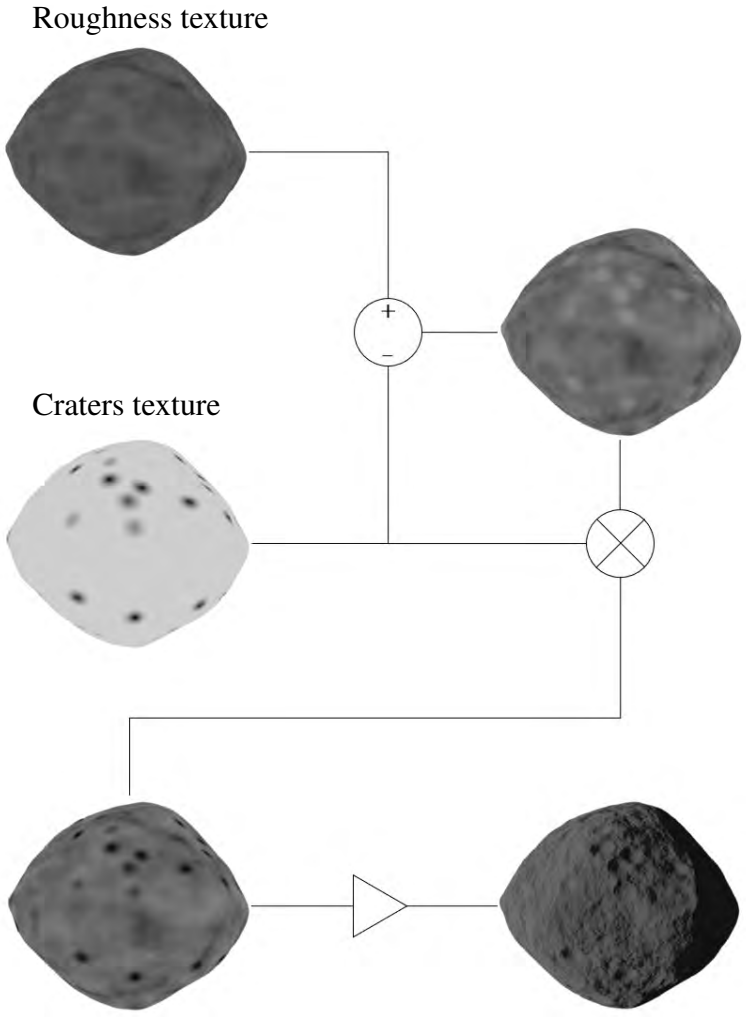

Fig. 6 Craters generation procedure. The operations performed on the textures are schematically reported along with the final result depicted on the bottom right. $\otimes$ represents the mix node multiplication, while $\triangleright$ is the bump node application.

[7] `https://docs.blender.org/manual/en/latest/render/shader_nodes/color/mix.html` Last Access: January 20, 2022

2.2.3 Boulders

Boulders are distributed over the surface of a minor body and their size can range from small to large. Fifty random rocks are created thanks to the *rock generator*[8] tool in Blender and the same material described in Section 2.2.1 is applied to each of them. This small number is selected to keep the computational burden low. However, the number of generated rocks are sufficient as they are placed on the body surface exploiting a particle system. As illustrated in Fig. 7, it is a particular Blender functionality, and it allows to duplicate and place objects on a surface if the "hair" type is selected. The number of particles or rocks can be chosen along with their size, phase angle and randomness. The last parameter is set up at the maximum value possible in order to get the most random configuration and avoid repetitions. In Fig. 7, a configuration with an elevated number of boulders is shown. As for the craters, a different number of particle systems can be generated, resulting in a large variety of boulders dimension, position, and orientation. By default, three different particle systems are set up, for small, medium, and large boulders.

In Fig. 8 the main building blocks of the Python code have been synthetically summarized, while in Fig. 9 a simplified version of the designed node tree for the introduction of craters and surface roughness on the minor body surface is presented. Finally, the entire procedural change process, from the rough 3D model to the refined one is depicted in Fig. 10.

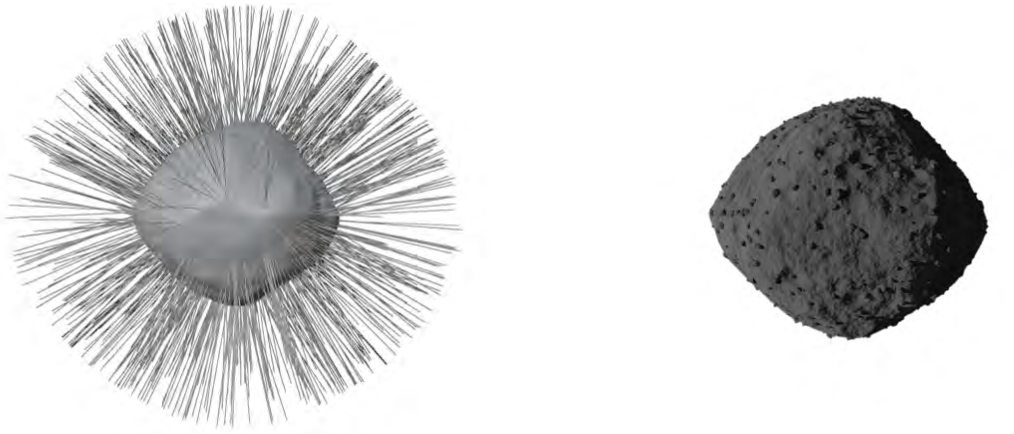

(a) **(b)**

Fig. 7 Boulders generation. (a) It is possible to see how the Blender's particle system works. (b) Final result with all the boulders placed on the surface of the model.

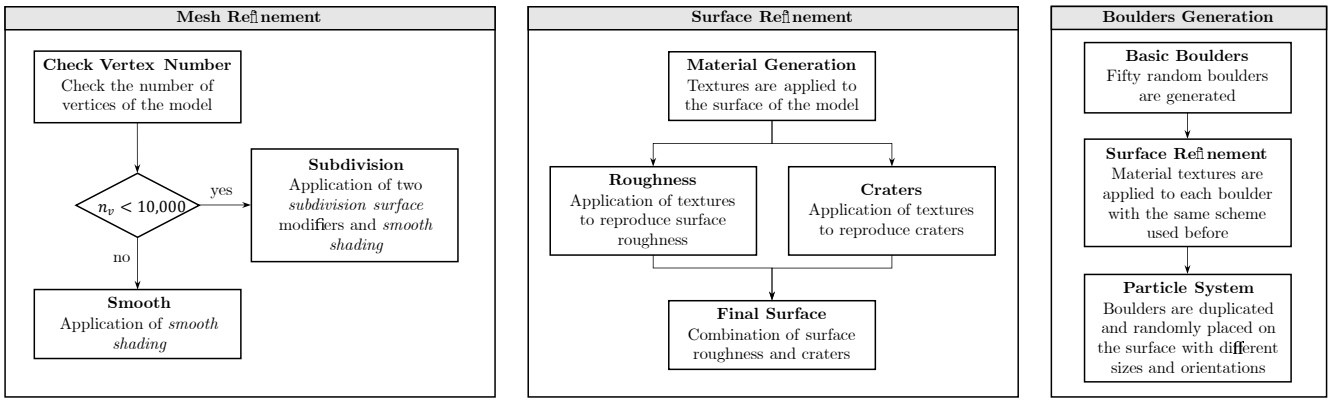

Fig. 8 Main building blocks of the Python script to procedurally modify minor bodies surface.

[8] `https://github.com/versluis/Rock-Generator` Last access: January 20, 2022

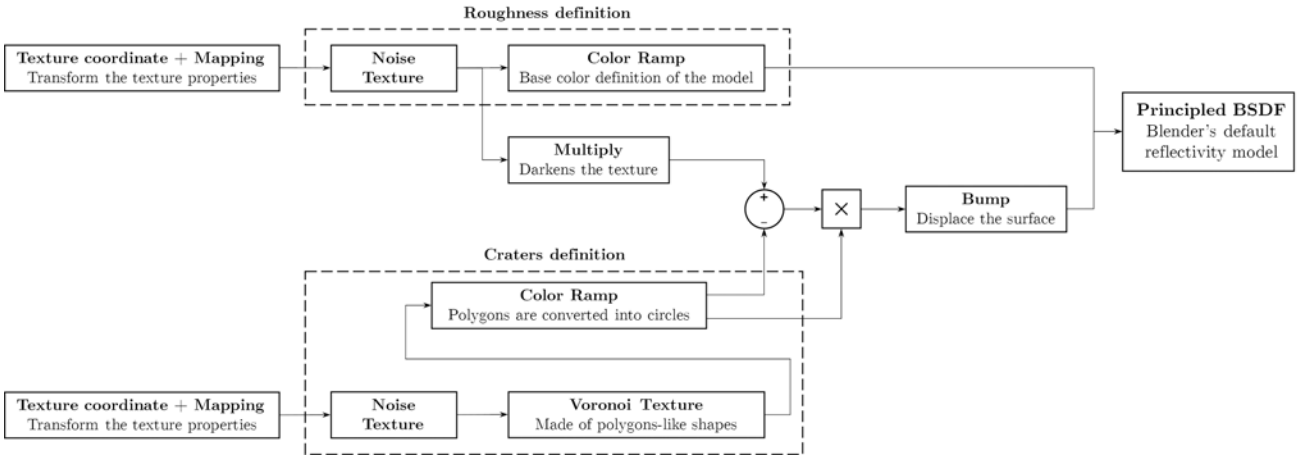

Fig. 9 Node tree associated to the surface refinement block for introducing surface roughness and craters.

2.3 Enviroment

In this section, the environment settings in Blender are specified, along with the rendering engine ones. The possibility to introduce optical aberrations is also briefly described.

2.3.1 Background

The background environment of a minor body consists of the presence of a light source (the Sun) and of a dark or stellar background.

The Sun light is directly available in Blender, and its direction and strength can be regulated. These are parameters that the user can change in order to get the most realistic scene possible.

Regarding the stars, they are easily obtained thanks to the *world* node tree characterized by a *noise* texture and a *color ramp* using black and white colors.

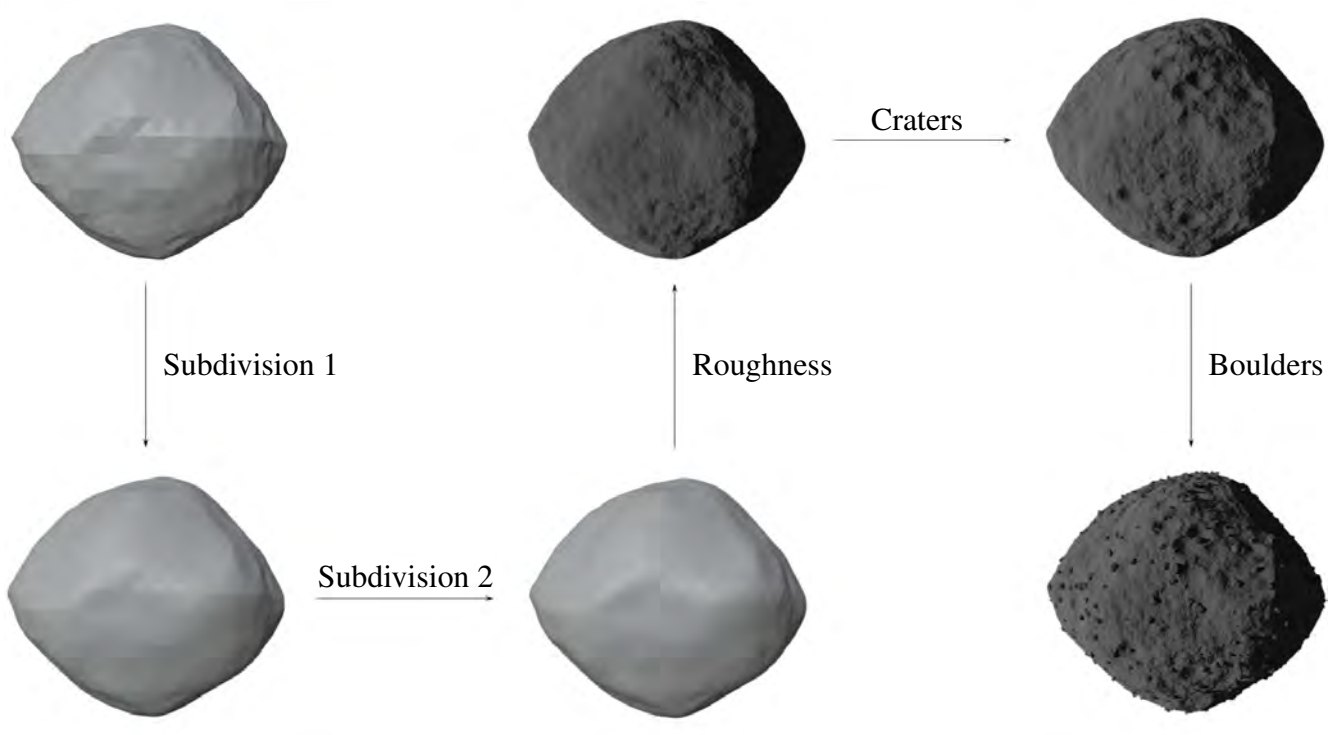

Fig. 10 Full process from the starting rough 3D model to the final refined one. First of all the mesh of the model is improved exploiting the Blender modifiers. Lately, a rough surface with craters and boulders is obtained.

2.3.2 Rendering

In Blender, the images are rendered in a simple way by placing a camera in a well suited position and selecting the rendering engine desired.
For this purpose, there are two main rendering engines:

- Eevee: a real time rendering engine which allows fast renders. It is usually used for long animations to ease the computational burden. Its main drawback is the need of optimization to make lights and shadows look correct.
- Cycles: the lights and shadows are much more realistic as it is an unbiased path-tracer rendering engine, which requires a higher computational effort.

The NVIDIA GTX 1050 Ti graphic card is exploited to run the renderings. The current implementation of the tool runs in Blender 2.83. With Cycles, a rendering sample of 128, and the default Blender camera at a distance of four times the average dimension of the model, about 120s are required to render an image. Clearly, the rendering time strongly depends on the user settings and on the camera distance: the closer the camera is to the model the longer is the rendering time. For what concerns the model surface properties, Blender's default reflectivity model, Principled BSDF (Bidirectional Scattering Distribution Function), is exploited and constant albedo is assumed.

2.3.3 Optical Aberrations

Optical aberrations can be considered exploiting the *compositing editor*[6] that could be used to post-process the rendered images and to introduce some errors by cameras.
Firstly, the body image can be blurred thanks to the *blur* node that provides several blur modes. Secondly, it is possible to introduce chromatic aberration that consists of the fact that rays of lights are bent at a different amount depending on their frequency. As a result the image can look blurred or noticeable colored edges can appear around the object. This effect is achieved thanks to the *lens distortion* node. *Glare* node allows the presence of light smearing caused by the reflection of the Sun light. In Tab. 1 all the default environment settings are reported.

Table 1 Default environment settings

Render	Engine	Cycles
	Integrator	Path Tracing
	Samples	128
Camera	Resolution	1024×1024 pxl
	Frame rate	24 fps
	Color	BW
	Color depth	8
	Compression	15%
Light	Type	Sun
	RGB color	(1,1,1)
	Strength	1
	Max bounces	1024

3 Results

In this section, different asteroid images realized with the tool are shown as a sample of its capability to generate a variety of models. In Figs. 11 and 12 it is possible to see images of the solar system's minor bodies that can be achieved with the tool. It should also be remarked that aberrations are not included and the models are those directly generated with the default settings. They can be further modified to make them even more realistic. In Fig. 11, two regular shaped bodies are rendered from the same perspective and lighting condition with increasing number of boulders. The image shows the tool capability in surface features generalization, in this case, by changing boulders number. Irregular and elongated shaped bodies are shown in Fig. 12, rendering them from three different perspectives and under various lighting conditions. It is possible to appreciate that the tool achieves real-looking rendering regardless of body shape, orientation, and illumination.

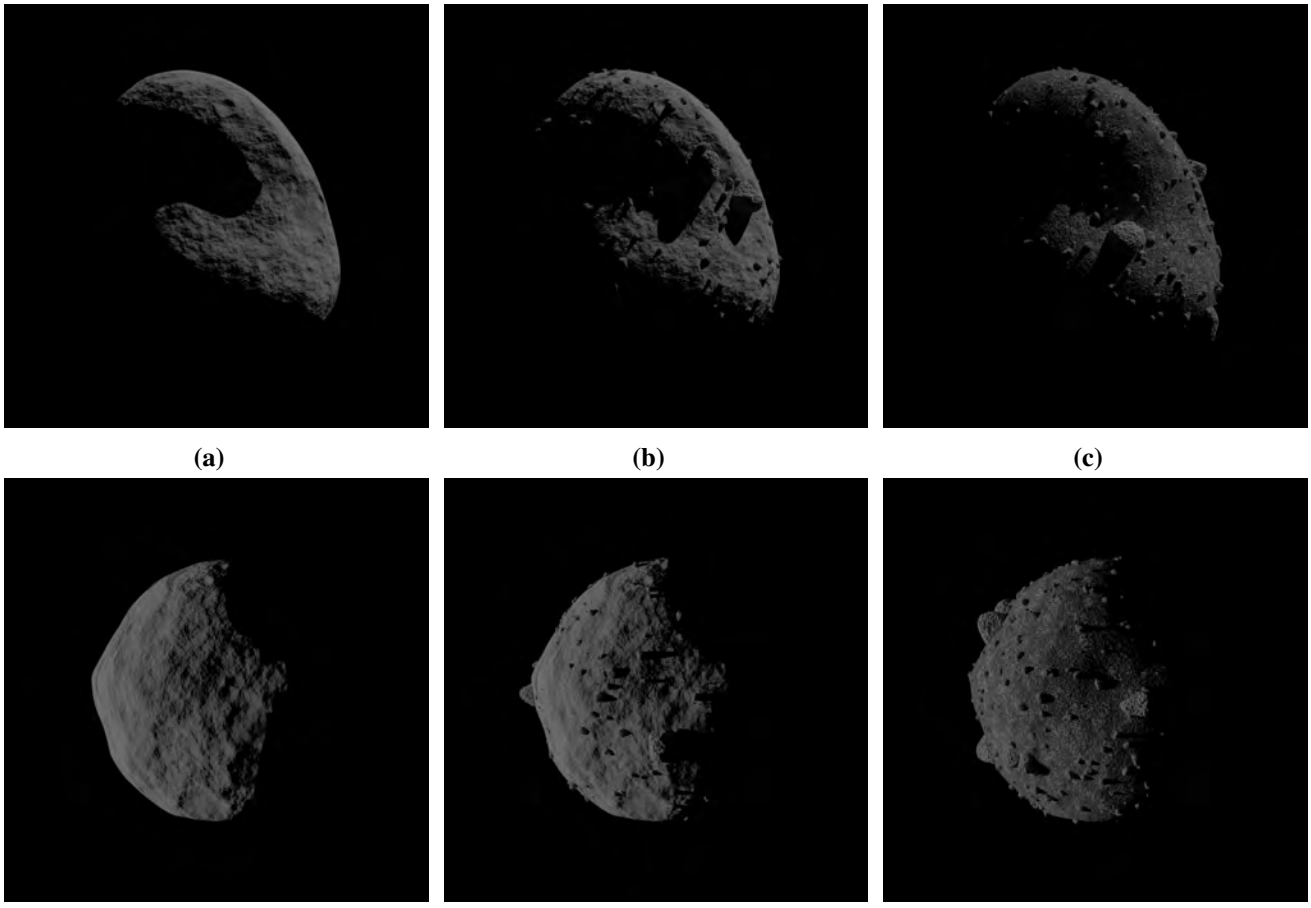

Fig. 11 Rendered images of asteroid Lutetia (from (a) to (c)) and Didymos (from (d) to (f)). By moving from left to right there is an increasing number of boulders: 0 small, 0 medium, 0 large in (a) and (d), 10,000 small, 400 medium, 3 large in (b) and (e), 300,000 small, 800 medium, 8 large in (c) and (f).

As already specified, the tool allows to generate two configurations of minor body surface features by default, which are the most common characteristics that have been found by visiting these bodies. The two families are distinguished only by a different parameters setting. In detail, the first family has 300,000 small rocks, 800 medium boulders, and a random number between 1 and 8 for large ones. Two craters types are defined, small and large ones, that are not clearly visible due to the massive presence of rocks that cover them. The second family consists of comet-like surface features, indeed it is characterized by the alternation of smooth and rough regions, achieved differently from the rocky body thanks to the multiplication of *musgrave* and *noise* textures in the surface roughness generation. These bodies are characterized by the scarce presence of craters, which are also small. The boulders are

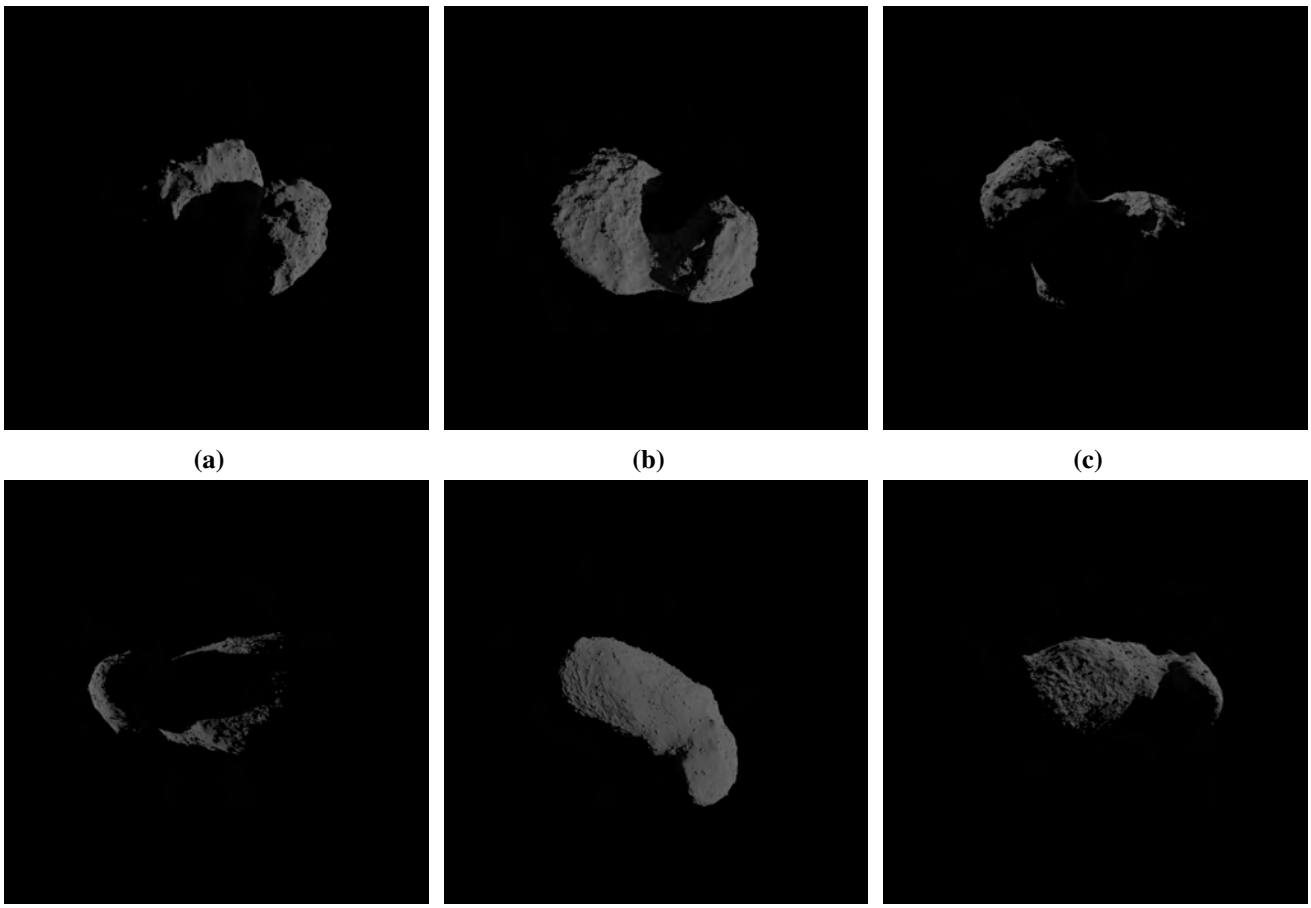

(a) **(b)** **(c)**

(d) **(e)** **(f)**

Fig. 12 Rendered images of two irregular shaped minor bodies from three different perspectives. From (a) to (c) comet 67p and from (d) to (f) asteroid Itokawa.

smaller in size with respect to the other family and their number is the following: 1000 small rocks, 100 medium boulders, and from 0 to 1 big ones. Some examples of the two families achieved with the tool are shown in Figs. 13 and 14, while a summary of the most important parameters characterizing them is given in Tab. 2.

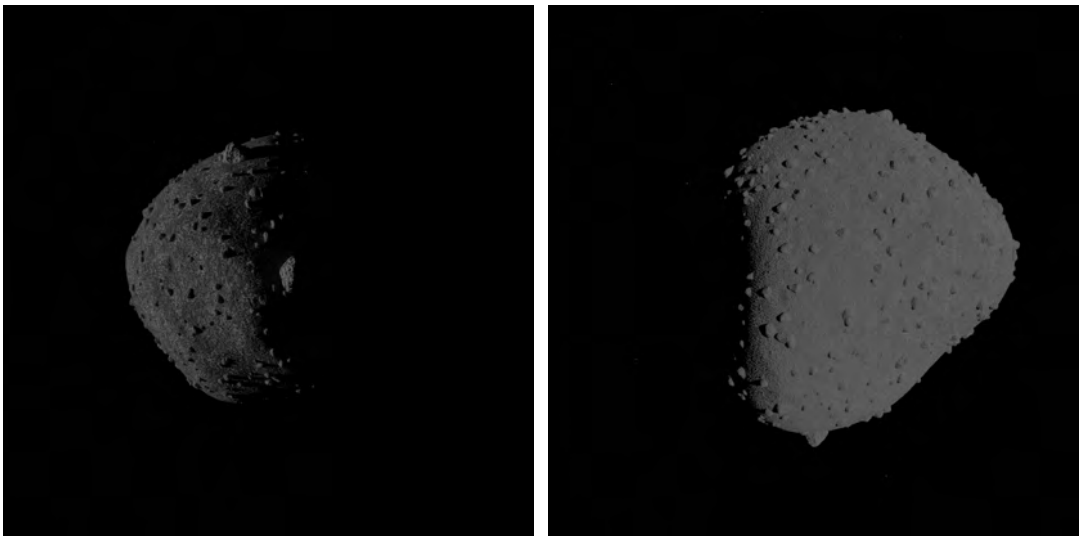

(a) **(b)**

Fig. 13 Rendered images with the surface morphological features of the first family. (a) Bennu (b) Thisbe.

Table 2 Minor bodies default families

		Rocky	**Comet-like**
Roughness	Texture	Noise	Noise and Musgrave
Craters	Dimension	Small and Large	Small
	Texture	Voronoi	Voronoi
Boulders	# Small	300,000	1,000
	# Medium	800	100
	# Large	1–8	0–1

(a) **(b)**

Fig. 14 Rendered images with the surface morphological features of the second family. (a) Itokawa (b) Eros.

3.1 Tool Validation

To validate the tool, it was tried to replicate an image of comet 67P taken by Rosetta's navigation camera (NavCam) at 21:50:13.052 on April 17, 2016 UTC. The raw processed image is shown in Fig. 15 and its features are clearly visible, as high resolution images are available since this comet has been studied extensively[9]. To get the same configuration, the comet's model was appropriately positioned in the camera view and the illumination conditions were set up in order to get the most similar lighting environment.
The image photorealism is achieved combining the highly realistic lighting environment in Blender with the tool's capability to obtain models very different from each other in terms of craters, rocks and surface morphology. The surface roughness appears like a real terrain thanks to its irregularities and non-periodicity as there are not unwanted repetitions. Boulders are not the main feature that it is noticed from images at elevated distances but they assume more and more importance the closer the camera gets. Although only 50 basic rocks have been generated, when multiple duplicates are placed on the surface, they seem all different from each other because of their various size and orientation. The craters' shape is slightly different from the circular one thanks to the *noise* texture applied on it. It must also be remarked that the photometric model used is the Principled BSDF. The use of more accurate photometric models [20] would result in an even more realistic image.

[9] `https://archives.esac.esa.int/psa/` Last access: January 20, 2022

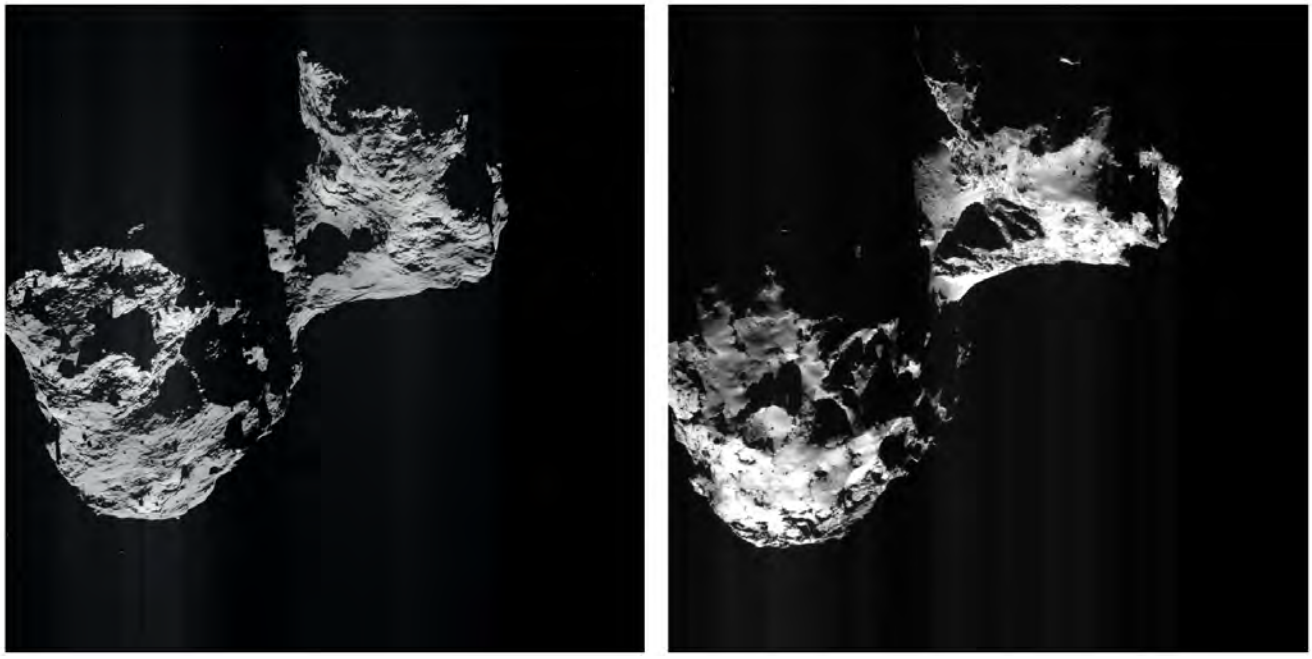

Fig. 15 Image reproduction of comet 67P taken during the Rosetta mission. In the image on the left there is the synthetic image generated with the tool while in the image on the right there is the actual comet photo taken by Rosetta's navigation camera (NavCam) at 21:50:13.052 on April 17, 2016 UTC.

4 Conclusions

In this work the design of the DART's minor bodies synthetic image generator tool, a Python code running on Blender used to create realistic minor body models in a real-looking environment is presented. This tool is used by the DART group to validate and test IP and VBN algorithms as well as to create large images dataset to feed artificial intelligence algorithms. The procedure to introduce surface morphology features such as roughness, craters, and boulders is illustrated. Families of small-bodies that can be achieved are presented as well as a validation assessment reproducing a real space image taken during the Rosetta mission of comet 67P. The authors believe such type of tools could be critical to assess VBN and IP performances for ongoing space missions [10, 21, 22] and projects of the DART's group.

Acknowledgments

M.P and F.T would like to acknowledge the funding received from the European Union's Horizon 2020 research and innovation programme under the Marie Skłodowska-Curie grant agreement No 813644.

References

[1] M. Quadrelli, L. Wood, J. Riedel, M. McHenry, M. Aung, L. Cangahuala, R. Volpe, P. Beauchamp, and J. Cutts. Guidance, Navigation, and Control Technology Assessment for Future Planetary Science Missions. *Journal of Guidance, Control, and Dynamics*, 38(7):1165–1186, 2015. DOI: 10.2514/1.G000525.

[2] D. S. Lauretta, S. S. Balram-Knutson, E. Beshore, W. V. Boynton, C. Drouet d'Aubigny, D. N. DellaGiustina, H. L. Enos, D. R. Golish, C. W. Hergenrother, E. S. Howell, C. A. Bennett, E. T. Morton, M. C. Nolan, B. Rizk, H. L. Roper, A. E. Bartels, B. J. Bos, J. P. Dworkin, D. E. Highsmith, D. A. Lorenz, L. F. Lim, R Mink, M. C. Moreau, J. A. Nuth, D. C. Reuter, A. A. Simon, E. B. Bierhaus, B. H. Bryan, R. Ballouz, O. S. Barnouin, R. P. Binzel, W. F. Bottke, V. E. Hamilton, K. J. Walsh, S. R. Chesley, P. R. Christensen, B. E. Clark, H. C. Connolly, M. K. Crombie, M. G. Daly, J. P. Emery, T. J. McCoy, J. W. McMahon, D. J. Scheeres, S. Messenger, K. Nakamura-Messenger, K. Righter, and S. A. Sandford. OSIRIS-REx: sample return from asteroid (101955) Bennu. *Space Science Reviews*, 212(1):925–984, 2017. DOI: 10.1007/s11214-017-0405-1.

[3] K. Glassmeier, H. Boehnhardt, D. Koschny, E. Kührt, and I. Richter. The Rosetta Mission: Flying Towards the Origin of the Solar System. *Space Science Reviews*, 128(1):1–21, 2007. DOI: 10.1007/s11214-9140-8.

[4] M. Yoshikawa, J. Kawaguchi, A. Fujiwara, and A. Tsuchiyama. Hayabusa Sample Return Mission. *Asteroids IV*, 1(397-418):1, 2015. DOI: 10.2458/azu_uapress_9780816532131-ch021.

[5] S. Watanabe, Y. Tsuda, M. Yoshikawa, S. Tanaka, T. Saiki, and S. Nakazawa. Hayabusa2 Mission Overview. *Space Science Reviews*, 208(1):3–16, 2017. DOI: 10.1007/s11214-017-0377-1.

[6] H. Levison, S. Marchi, K. Noll, C. Olkin, and T. Statler. NASA's Lucy Mission to the Trojan Asteroids. In *IEEE Aerospace Conference (50100)*, 2021.

[7] P. Michel, M. Kueppers, H. Sierks, I. Carnelli, A. F. Cheng, K. Mellab, M. Granvik, M. Kestilä, T. Kohout, K. Muinonen, A. Näsilä, A. Penttila, T. Tikka, P. Tortora, V. Ciarletti, A. Hérique, N. Murdoch, E. Asphaug, A. Rivkin, O. Barnouin, A. C. Bagatin, P. Pravec, D. C. Richardson, S. R. Schwartz, K. Tsiganis, S. Ulamec, and O. Karatekin. European Component of the AIDA Mission to a Binary Asteroid: Characterization and Interpretation of the Impact of the DART Mission. *Advances in Space Research*, 62(8):2261–2272, 2018. DOI: 10.1016/j.asr.2017.12.020.

[8] M. Pugliatti, A. Rizza, F. Piccolo, V. Franzese, C. Bottiglieri, C. Giordano, F. Ferrari, and F. Topputo. The Milani Mission: Overview and Architecture of the Optical-Based GNC System. In *AIAA SCITECH 2022 Forum*, 2022.

[9] H. Goldberg, Ö. Karatekin, B. Ritter, A. Herique, P. Tortora, C. Prioroc, B. G. Gutierrez, P. Martino, and I. Carnelli. The Juventas CubeSat in Support of ESA's Hera Mission to the Asteroid Didymos. In *33rd Annual AIAA/USU Conference on Small Satellites*, 2019.

[10] F. Topputo, Y. Wang, C. Giordano, V. Franzese, H. Goldberg, F. Perez-Lissi, and R. Walker. Envelop of Reachable Asteroids by M-ARGO CubeSat. *Advances in Space Research*, 67(12):4193–4221, 2021. DOI: 10.1016/j.asr.2021.02.031.

[11] D. J. Scheeres. *Orbital Motion in Strongly Perturbed Environments: Applications to Asteroid, Comet and Planetary Satellite Orbiters*. Springer, 2016.

[12] C. Buonagura. Image processing robustness assessment with procedural generated minor bodies shapes. Master's thesis, Politecnico di Milano, 12 2020. Accessible from: `https://www.politesi.polimi.it/handle/10589/175354`.

[13] M. Pugliatti, V. Franzese, and F. Topputo. Data-Driven Image Processing for Onboard Optical Navigation Around a Binary Asteroid. *Journal of Spacecraft and Rockets*, 1:1–17, 2022. DOI: 10.2514/1.A35213.

[14] N. Rowell, S. Parkes, M. Dunstan, and O. Dubois-Matra. PANGU: Virtual spacecraft image generation. 2012.

[15] J. Lebreton, R. Brochard, M. Baudry, Grégory J., Adrien H. S., K. Kanani, M. L. Goff, A. Masson, N. Ollagnier, P. Panicucci, A. Proag, and C. Robin. Image simulation for space applications with the SurRender software. In *11th International ESA Conference on Guidance, Navigation & Control Systems*, 2021.

[16] M. Pugliatti, M. Maestrini, P. Di Lizia, and F. Topputo. Onboard Small-Body Semantic Segmentation Based on Morphological Features with U-Net. In *31st AAS/AIAA Space Flight Mechanics Meeting*, 2021.

[17] K. J. Walsh, E. R. Jawin, R.-L. Ballouz, O. S. Barnouin, E. B. Bierhaus, H. C. Connolly, J. L. Molaro, T. J. Mccoy, M. Delbo, C. Hartzell, M. Pajola, S. R. Schwartz, D. Trang, E. Asphaug, K. J. Becker, C. B. Beddingfield, C. A. Bennett, W. F. Bottke, K. N. Burke, B. C. Clark, M. G. Daly, D. N. DellaGiustina, J. P. Dworkin, C. M. Elder, D. R. Golish, A. R. Hildebrand, R. Malhotra, J. R. Marshall, P. Michel, M. C. Nolan, M. E. Perry, B. Rizk, A. J. Ryan, S. A. Sandford, D. J. Scheeres, H. C. M. Susorney, F. Thuillet, and D. S. Lauretta. Craters, Boulders and Regolith of (101955) Bennu Indicative of an Old and Dynamic Surface. *Nature Geoscience*, 12(4):242–246, 2019. DOI: 10.1038/s41561-019-0326-6.

[18] M. R. El-Maarry, N. Thomas, L. Giacomini, M. Massironi, M. Pajola, R. Marschall, A. Gracia-Berná, H. Sierks, C. Barbieri, P. L. Lamy, R. Rodrigo, H. Rickman, D. Koschny, H. U. Keller, J. Agarwal, M. F. A´Hearn, A.-T. Auger, M. A. Barucci, J.-L. Bertaux, I. Bertini, S. Besse, D. Bodewits, G. Cremonese, V. Da Deppo, B. Davidsson, M. De Cecco, S. Debei, C. Güttler, S. Fornasier, M. Fulle, O. Groussin, P. J. Gutierrez, S. F. Hviid, W.-H. Ip, L. Jorda, J. Knollenberg, G. Kovacs, J.-R. Kramm, E. Kührt, M. Küppers, F. La Forgia, L. M. Lara, M. Lazzarin, J. J. Lopez Moreno, S. Marchi, F. Marzari, H. Michalik, G. Naletto, N. Oklay, A. Pommerol, F. Preusker, F. Scholten, C. Tubiana, and J.-B. Vincent. Regional Surface Morphology of Comet 67P/Churyumov-Gerasimenko from Rosetta/OSIRIS Images. *Astronomy & Astrophysics*, 583:A26, 2015. DOI: 10.1051/0004-6361/201525723.

[19] E. Catmull and J. Clark. Recursively generated B-spline surfaces on arbitrary topological meshes. *Computer-aided design*, 10(6):350–355, 1978. DOI: https://doi.org/10.1016/0010-4485(78)90110-0.

[20] D. R. Golish, D. N. DellaGiustina, J.-Y. Li, B. E. Clark, X.-D. Zou, P. H. Smith, J. L. Rizos, P. H. Hasselmann, C. A. Bennett, S. Fornasier, R.-L. Ballouz, C. Drouet d'Aubigny, B. Rizk, M. G. Daly, O. S. Barnouin, L. Philpott, M. M. Al Asad, J. A. Seabrook, C. L. Johnson, and D. S. Lauretta. Disk-resolved photometric modeling and properties of asteroid (101955) Bennu. *Icarus*, 357:113724, 2021. DOI: https://doi.org/10.1016/j.icarus.2020.113724.

[21] V. Franzese, P. Di Lizia, and F. Topputo. Autonomous Optical Navigation for the Lunar Meteoroid Impacts Observer. *Journal of Guidance, Control, and Dynamics*, 42(7):1579–1586, 2019. DOI: 10.2514/1.G003999.

[22] F. Ferrari, V. Franzese, M. Pugliatti, C. Giordano, and F. Topputo. Preliminary Mission Profile of Hera's Milani CubeSat. *Advances in Space Research*, 67(6):2010–2029, 2021. DOI: 10.1016/j.asr.2020.12.034.